



Nanog signaling in cancer promotes stem-like phenotype and immune evasion

Kyung Hee Noh,¹ Bo Wook Kim,² Kwon-Ho Song,¹ Hanbyoul Cho,³ Young-Ho Lee,¹ Jin Hee Kim,¹ Joon-Yong Chung,² Jae-Hoon Kim,³ Stephen M. Hewitt,² Seung-Yong Seong,⁴ Chih-Ping Mao,⁵ T.-C. Wu,^{5,6,7,8} and Tae Woo Kim¹

¹Division of Infection and Immunology, Graduate School of Medicine, Korea University, Seoul, Republic of Korea. ²Tissue Array Research Program and Applied Molecular Pathology Laboratory, Laboratory of Pathology, Center for Cancer Research, National Cancer Institute, NIH, Bethesda, Maryland, USA.

³Department of Obstetrics and Gynecology, Gangnam Severance Hospital, Yonsei University College of Medicine, Seoul, Republic of Korea.

⁴Department of Microbiology and Immunology, Seoul National University College of Medicine, Seoul, Republic of Korea.

⁵Department of Pathology, ⁶Department of Obstetrics and Gynecology, ⁷Department of Oncology,

and ⁸Department of Molecular Microbiology and Immunology, Johns Hopkins School of Medicine, Baltimore, Maryland, USA.

Adaptation of tumor cells to the host is a major cause of cancer progression, failure of therapy, and ultimately death. Immune selection drives this adaptation in human cancer by enriching tumor cells with a cancer stem cell-like (CSC-like) phenotype that makes them resistant to CTL-mediated apoptosis; however, the mechanisms that mediate CSC maintenance and proliferation are largely unknown. Here, we report that CTL-mediated immune selection drives the evolution of tumor cells toward a CSC-like phenotype and that the CSC-like phenotype arises through the Akt signaling pathway via transcriptional induction of Tc1a by Nanog. Furthermore, we found that hyperactivation of the Nanog/Tc1a/Akt signaling axis was conserved across multiple types of human cancer. Inhibition of Nanog in a murine model of colon cancer rendered tumor cells susceptible to immune-mediated clearance and led to successful, long-term control of the disease. Our findings establish a firm link among immune selection, disease progression, and the development of a stem-like tumor phenotype in human cancer and implicate the Nanog/Tc1a/Akt pathway as a central molecular target in this process.

Introduction

Despite heroic efforts by humankind to combat cancer over millennia, this disease remains the second leading cause of death in the United States, afflicting approximately 50% of all men and 30% of all women (1). It is now clear that a central reason that a cure for cancer has thus far been elusive is the constant adaptation of tumor cells to the defenses – internal – mounted by the host they inhabit (2–4). For example, conventional interventions, such as radiation or chemotherapy, may eliminate the bulk of the tumor but spare highly aggressive cancer cells that have an exceptional capacity to survive, self-renew, and advance the malignancy (5–7). These residual cells have recently been found to possess key stem-like attributes and have thus been coined “cancer stem cells” (CSCs) (8–10). CSCs are believed to be primarily responsible for tumor progression, metastasis, and relapse after therapy (11–13). The existence and persistence of these cells may therefore explain the failure of current cancer treatment modalities.

The dynamics of CSC maintenance and propagation remain largely unknown. Transformed cells are continuously subjected to immune selection; cells that can survive immune attack are preferentially retained, while those that cannot are eradicated (3). We have recently shown, in a mouse model of cervical carcinoma, that a vaccination regimen which induces CTL-mediated immune selection drives the evolution of tumor cells toward a stem-like and antiapoptotic phenotype in a process that requires the Nanog transcription factor (14). This finding argues that immune selec-

tion can be a perpetuating force for cancer progression. However, the molecular mechanism by which Nanog mediates immune escape and the relevance of Nanog expression in human cancer have not been previously explored. Both of these issues are essential for clinical translation and form the premise of this study.

Here, we demonstrate for the first time to our knowledge that immune selection of human cancer cells causes enrichment of a subset of cells with high Nanog expression. These cells exhibit stem-like, antiapoptotic properties and are impervious to immune attack. Importantly, the phenotype of these cells is critically dependent on Nanog, which, through its transcriptional activity, triggers the T cell leukemia/lymphoma 1A/Akt (Tc1a/Akt) signaling axis. We report that Nanog expression in tumor tissue is correlated with the stage of disease and prognosis of patients with cervical neoplasia. Furthermore, we found that Nanog overexpression – as well as the stem-like, antiapoptotic tumor phenotype this protein promotes – is conserved across multiple types of human cancer. Finally, we provide proof of the principle in a preclinical model that Nanog inhibition is an effective strategy to control human cancer, particularly in the context of immune-based therapy.

Results

Immune selection enhances the growth and stem-like properties of tumor cells. We applied in vitro immune selection to generate human tumor cells impervious to lysis by antigen-specific CTLs, as illustrated in Figure 1A. Human cervical cancer cells from the CaSki line (designated P0 cells) were retrovirally transduced with the mouse major histocompatibility complex (MHC) class I molecule H2-D^b, pulsed with the H2-D^b-restricted E7 epitope from human papillomavirus type 16, and mixed with mouse E7-specific CTLs. The live tumor cells were recovered as the P1 line. Further rounds of selection were used to generate the P2 and P3

Authorship note: Kyung Hee Noh, Bo Wook Kim, Kwon-Ho Song, and Hanbyoul Cho contributed equally to this work.

Conflict of interest: The authors have declared that no conflict of interest exists.

Citation for this article: *J Clin Invest.* 2012;122(11):4077–4093. doi:10.1172/JCI64057.

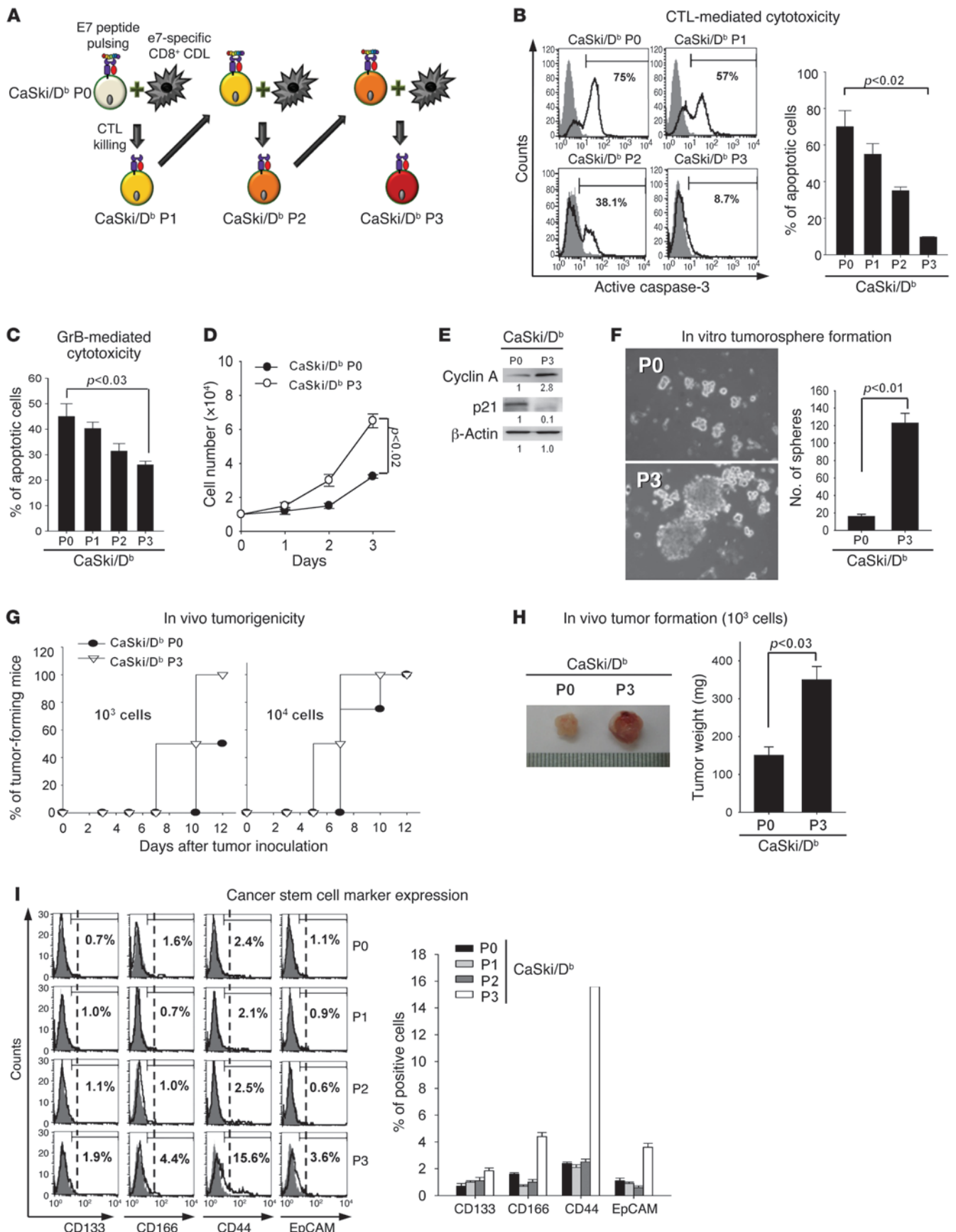




Figure 1

Immune selection enhances the stem-like properties and tumorigenicity of human cancer cells. **(A)** Diagram depicting the process of in vitro immune selection of human cervical cancer cells. **(B and C)** Flow cytometry analysis of the frequency of apoptotic (active caspase-3⁺) cells in the P0, P1, P2, and P3 populations **(B)** after incubation with E7-specific CTLs at a 1:1 ratio for 4 hours (isotype control staining is indicated by solid gray regions; anti-active caspase-3 staining is indicated by the black lines) or **(C)** after intracellular delivery of granzyme B. **(D)** Growth rate of P0 versus P3 cells in culture. Cells were harvested at the indicated times and counted after trypan blue staining to exclude dead cells. **(E)** Western blot analysis of expression of cyclin A and p21 in P0 versus P3 cells. β -Actin was included as an internal loading control. Numbers below blots indicate expression as measured by fold change. **(F)** Sphere-forming capacity of P0 versus P3 cells in low-density suspension culture. Original magnification, $\times 40$. **(G)** Tumorigenicity of P0 versus P3 cells inoculated at indicated doses into 5 NOD/SCID mice per group. **(H)** Tumor burden 12 days after injection of 10^3 P0 or P3 cells. **(I)** Flow cytometry analysis of stemness markers in P0, P1, P2, and P3 populations (isotype control staining is indicated by solid gray region; staining for stemness markers is indicated by black lines). Error bars represent mean \pm SD.

populations, which were sequentially more resistant to lysis by antigen-specific CTLs or granzyme B, as demonstrated by the frequency of active caspase-3⁺ cells (Figure 1, B and C). Notably, over 90% of P3 cells survived when mixed with CTLs, compared with only 10% of the P0 cells (Figure 1B). Relative to the P0 cells, the P3 cells also proliferated more quickly (Figure 1D) and had nearly 3-times more cyclin A and 10-times less p21 expression (Figure 1E).

In addition to displaying a faster growth rate, the P3 cells exhibited a stem-like phenotype. These cells readily formed spheres when cultured under suspension conditions (Figure 1F) and were more tumorigenic than the parental P0 line when transplanted into NOD/SCID mice (Figure 1, G and H). Furthermore, the P3 population was enriched in cells expressing a panel of stemness markers. For example, compared with P0 cells, there were about 3-times more P3 cells expressing CD133, CD166, or EpCAM (Figure 1I). There were 7-times more P3 cells than P0 cells expressing CD44 (Figure 1I). Thus, these data indicate that immune selection increases the growth rate and stem-like phenotype of human tumor cells, consistent with what has been reported for other types of conventional cancer treatment, such as chemotherapy or radiation therapy (5–7).

Immune selection enriches Nanog-expressing tumor cells. To examine the molecular basis for the enhanced growth rate and stem-like phenotype of tumor cells following immune selection, we assessed the expression of a set of stemness markers from the P0, P1, P2, and P3 populations. Among these markers, we only found a substantial difference in Nanog expression among the various populations (Figure 2A). Specifically, Nanog accumulated with sequential rounds of immune selection, and the total level of Nanog protein was 3-fold higher in P3 cells than in P0 cells (Figure 2A). The overall increase in Nanog expression in the P3 line was likely due to enrichment of Nanog⁺ cells, as opposed to upregulation of Nanog, since the frequency of Nanog⁺ cells rose from around 5% in the P0 line to around 90% in the P3 line (18-fold enrichment) (Figure 2B). It is possible that the mere presence of CTLs in culture with tumor cells exerts metabolic stress that enriches Nanog⁺ cells. To exclude this possibility, we

performed selection by mixing CaSki-H2-D^b cells pulsed with either E7 or irrelevant (Ova) peptide together with E7-specific T cells. While CaSki-H2-D^b cells loaded with E7 peptide are subjected to both immune attack and metabolic stress, those loaded with Ova peptide are subjected only to metabolic stress. We measured Nanog levels in the tumor cells after sequential rounds of selection and found that Nanog expression increased after selection with E7 but not with Ova peptide (Supplemental Figure 1; supplemental material available online with this article; doi:10.1172/JCI64057DS1). Furthermore, we did not observe Nanog upregulation or development of an immune-resistant phenotype after mixing E7 peptide-pulsed CaSki-H2-D^b cells with irrelevant Ova-specific CD8⁺ T cells for several cycles (data not shown). Therefore, we conclude that metabolic stress does not contribute to the development of a stem-like and immune-resistant phenotype in tumor cells under immune selection. Thus, immune selection depletes cells lacking Nanog and spares those containing Nanog in an antigen-specific manner. This suggests that Nanog may confer a growth and survival advantage to tumor cells and may promote the formation of cells resembling CSCs.

Nanog is critical for the augmented growth and stem-like properties of immune-selected tumor cells. To test this possibility, we treated P3 cells with siRNA-targeting Nanog (siNanog) or siRNA-targeting GFP (siGFP) control. We observed that administration of siNanog reduced by over 2-fold the frequency of CD133⁺ or CD44⁺ P3 cells (Figure 2D). Furthermore, siNanog decreased cyclin A protein levels by 10 fold and increased p21 levels by 5.3 fold in the P3 line (Figure 2C). Consistent with these changes in protein levels, siNanog-treated cells proliferated more slowly, formed over 3-times fewer spheres, and contained nearly 4-times more apoptotic cells when mixed with E7-specific CTLs compared with siGFP-treated cells (Figure 2, E–G). Taken together, our data indicate that Nanog provides a growth and survival advantage to tumor cells and contributes to their stem-like phenotype.

It is conceivable that Nanog expression in tumor cells influences the antigen-processing or -presentation pathway, which could account for decreased sensitivity to lysis by CTLs. Therefore, we assessed (a) MHC class I (H2-D^b) expression in CaSki-H2-D^b cells transduced with empty vector or Nanog and (b) the presentation of E7 peptide through MHC class I to E7-specific CD8⁺ T cells. We found that both MHC class I expression and presentation of E7 peptide to E7-specific CD8⁺ T cells were virtually identical, regardless of Nanog expression status in tumor cells (Supplemental Figure 2). Thus, we conclude that Nanog in tumor cells does not influence MHC class I expression or antigen presentation by tumor cells.

We next tested the possibility that Nanog expression in tumor cells may alter the functional capacity or survival of antigen-specific CTLs. We found there was no difference in CTL effector cytokine (IFN- γ) production, tumor surface expression of the apoptosis-inducing molecule Fas ligand, or survival of E7-specific CTLs mixed with E7-loaded tumor cells, regardless of Nanog expression (Supplemental Figures 2 and 3). Thus, we conclude that Nanog expression in tumor cells renders these cells impervious to lysis by CTLs but does not affect the intrinsic functional capacity of the CTLs.

Nanog promotes an immune-resistant and stem-like phenotype in tumor cells through Akt-dependent upregulation of Mcl-1. We next sought to determine the mechanism by which Nanog confers a growth and survival advantage, as well as a stem-like phenotype, to tumor cells.

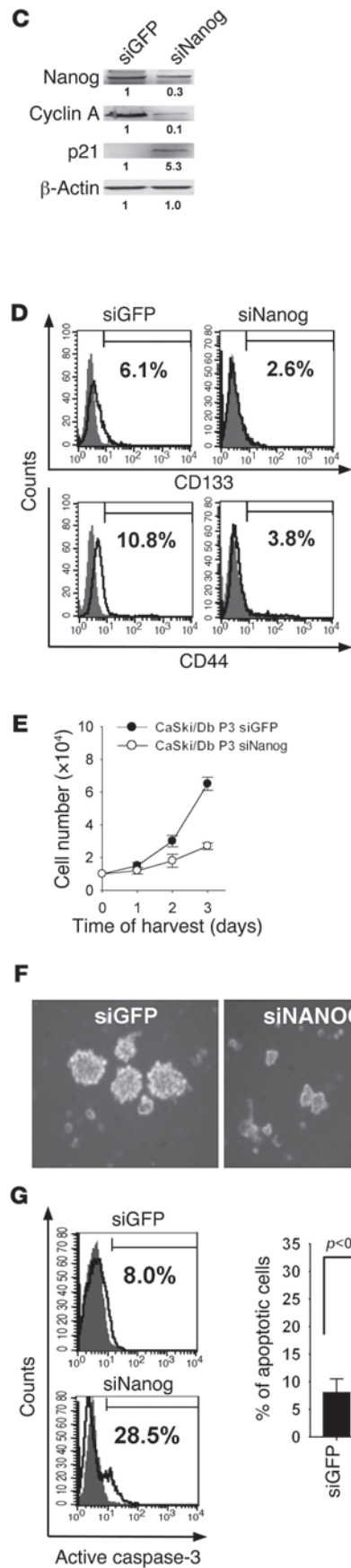
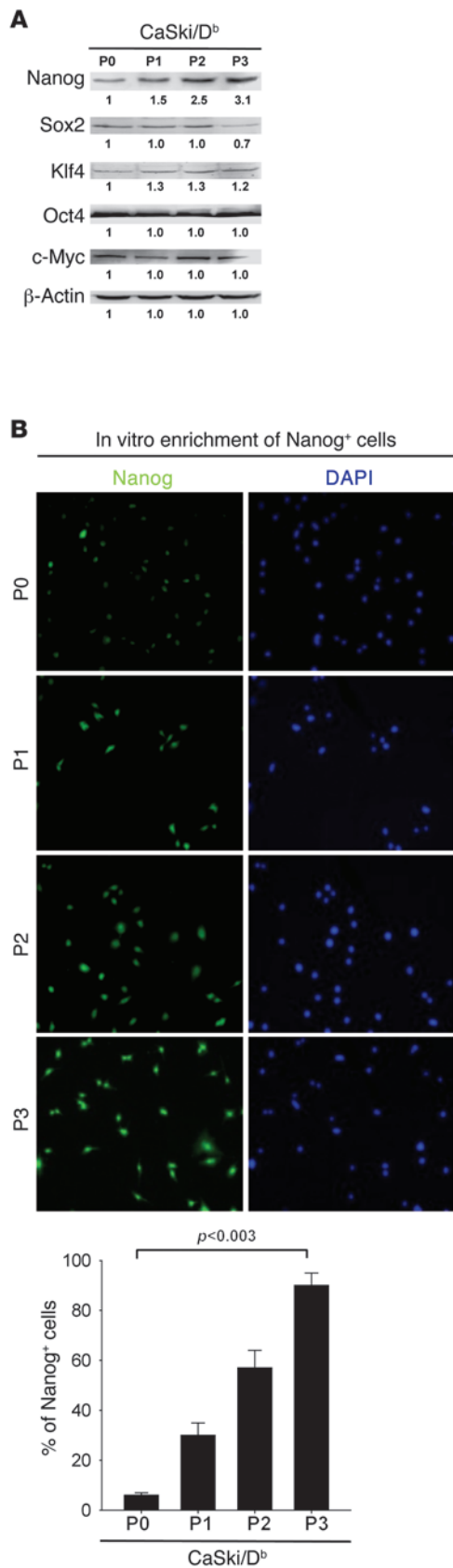


Figure 2

Nanog confers stem-like properties as well as a growth and survival advantage to immune-selected human cancer cells. **(A)** Western blot analysis of a panel of stemness factors in P0, P1, P2, and P3 populations. β-Actin was included as an internal loading control. **(B)** Immunofluorescence analysis of the frequency of Nanog⁺ cells in P0, P1, P2, and P3 populations. β-Actin was included as an internal loading control. **(C)** Western blot analysis of Nanog, cyclin A, and p21 expression in P3 cells treated with siGFP or siNanog. β-Actin was used as an internal loading control. **(D)** Flow cytometry analysis of stemness marker (CD133 and CD44) expression in siGFP- or siNanog-treated P3 cells. **(E)** Growth rate of siGFP- versus siNanog-treated P3 cells in culture. Cells were harvested at the indicated times and counted after trypan blue staining to exclude dead cells. **(F)** Sphere-forming capacity of siGFP- versus siNanog-treated P3 cells in low-density suspension culture. **(G)** Flow cytometry analysis of the frequency of apoptotic (active caspase-3⁺) cells in the P0, P1, P2, and P3 populations after incubation with E7-specific CTLs at a 1:1 ratio for 4 hours (isotype control staining is indicated by solid gray region; anti-active caspase-3 staining is indicated by black lines). **(A** and **C)** Numbers below blots indicate expression as measured by fold change. Error bars represent mean ± SD. Original magnification, ×40.

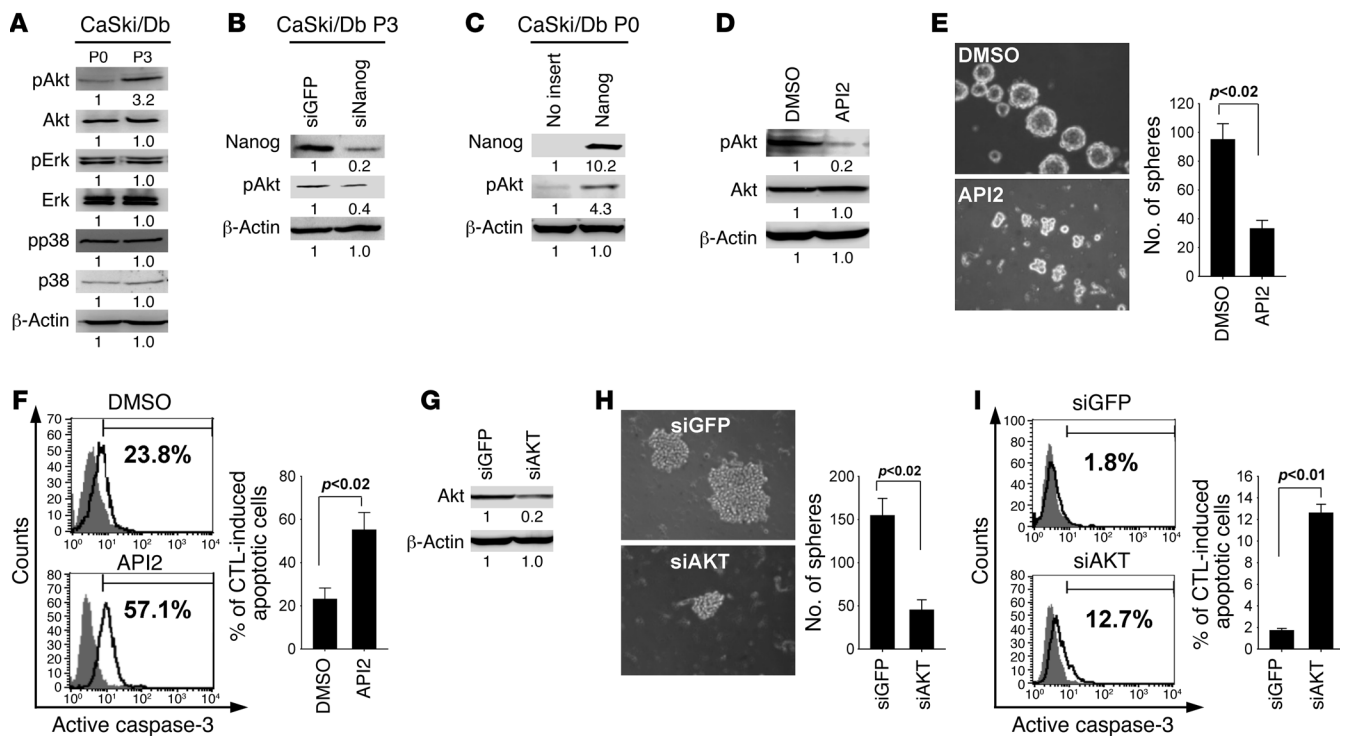


Figure 3

Nanog promotes the stem-like and immune-resistant phenotype of tumor cells through the Akt pathway. (A–C) Western blot analysis of expression and activation status (A) of a panel of major signaling molecules in P0 or P3 cells or (B) of Nanog and pAkt expression in P3 cells treated with siGFP or siNanog or (C) in empty vector– or Nanog cDNA–transfected P0 cells. β-Actin was included as an internal loading control. (D and G) Western blot analysis of pAkt or total Akt levels in Nanog-transfected P0 cells treated with either (D) API2 and DMSO control or (G) siAkt and siGFP control. (E and H) Sphere-forming capacity of Nanog-transfected P0 cells treated with either (E) API2 and DMSO control or (H) siAkt and siGFP control. Original magnification, ×40. (F and I) Flow cytometry analysis of the frequency of apoptotic (active caspase-3⁺) cells in Nanog-transfected P0 cells treated with either (F) API2 and DMSO control or (I) siAkt and siGFP control after incubation with E7-specific CTLs at a 1:1 ratio for 4 hours (isotype control staining is indicated by solid gray region; anti-active caspase-3 staining is indicated by black lines). (A–D and G) Numbers below blots indicate expression as measured by fold change. Error bars represent mean ± SD.

We assessed the status of a panel of important signaling cascades – including those controlled by Akt, Erk, and p38 – in P0 cells compared with that in P3 cells. Among these, we found the phosphorylation of Akt to be 3-times higher in P3 cells than in P0 cells (Figure 3A). We then asked whether phosphorylation of Akt in P3 cells is mediated through Nanog. Interestingly, delivery of siNanog into P3 cells reduced Akt phosphorylation by over 2 fold. Conversely, introduction of Nanog into P0 cells increased Akt phosphorylation by over 4 fold (Figure 3, B and C). To explore the relationship between the Nanog-induced stem-like phenotype and the Akt pathway, we treated Nanog-transduced P0 cells with API2, an inhibitor of Akt phosphorylation, or DMSO control (Figure 3D). API2-treated Nanog⁺ cells formed 3-times fewer spheres and contained almost 3-times more apoptotic cells compared with DMSO-treated Nanog⁺ cells (Figure 3, E and F). To exclude potential off-target effects of API2, we performed the same experiment using siRNA-targeting Akt (siAkt) to block the Akt pathway and observed similar results (Figure 3, G–I). Thus, our data indicate that Nanog mediates the pro-survival and stem-like phenotype of tumor cells through the Akt pathway.

Because Nanog regulates multiple gene expression programs critical for self-renewal of stem cells, we asked whether Nanog mediates its effects through its transcriptional function. To address this, we engineered a mutant form of Nanog (Nanog MT)

cDNA in which the CD2 domain – known to be pivotal for its transcriptional function (15, 16) – contains 3 inactivating point mutations (E264G, E268G, and E272A) (ref. 16 and Supplemental Figure 4A). P0 cells transfected with Nanog MT, relative to those transfected with wild-type Nanog (Nanog WT), had reduced expression of a luciferase reporter gene introduced under the control of Nanog-binding elements in the pGL3-5×NBE construct (Supplemental Figure 4B).

P0 cells transfected with Nanog MT, in contrast with those transfected with Nanog WT, failed to markedly increase phosphorylation of Akt or change expression levels of cyclin A or p21 (Figure 4, A and B). Moreover, while addition of Nanog WT accelerated the growth and improved the sphere-forming capacity of P0 cells, addition of Nanog MT had no substantial impact on these parameters (Figure 4, C and D). Also, delivery of Nanog WT to P0 cells reduced lysis by CTLs by over 80%, while delivery of Nanog MT did not significantly alter the susceptibility of P0 cells to lysis (Figure 4E).

We reasoned that the enhanced growth, survival, and immune resistance conferred by Nanog may be due to its effects on proteins involved in the apoptotic pathway. We thus measured the expression levels of a panel of proapoptotic or antiapoptotic proteins. Notably, the amount of the antiapoptotic molecule Mcl-1 was elevated 3 fold in Nanog WT-transfected cells and slightly in Nanog

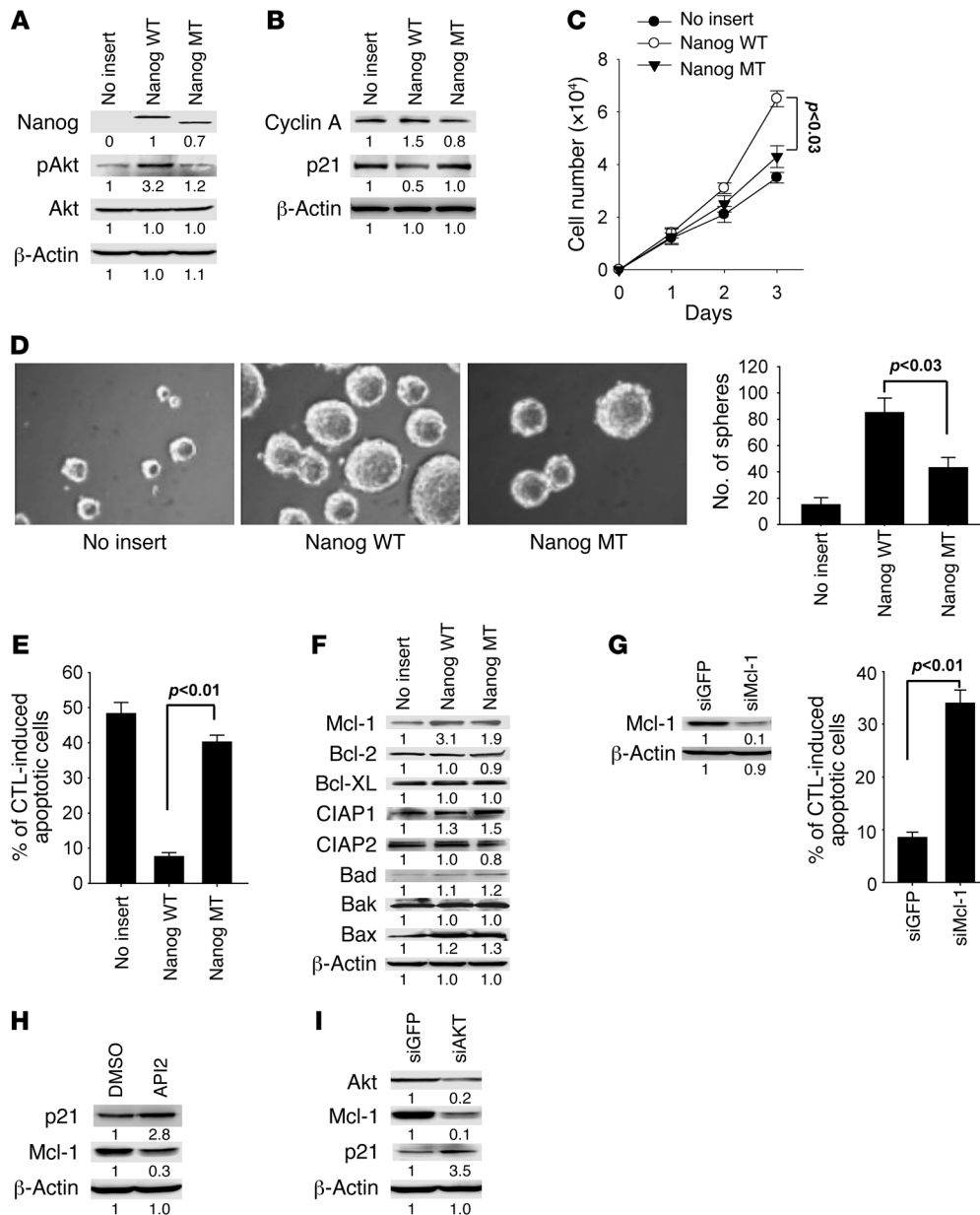


Figure 4

The transcriptional function of Nanog is required for it to induce a stem-like phenotype and activate an antiapoptotic program in human cancer cells. (A and B) Western blot analysis of (A) Nanog, pAkt, or Akt as well as (B) cyclin A or p21 expression in P0 cells transfected with either Nanog WT or Nanog MT cDNA. (C) Growth rate of Nanog WT–transfected cells versus that of Nanog MT–transfected cells in culture. (D) Sphere-forming capacity of Nanog WT–transfected P0 cells versus that of Nanog MT–transfected P0 cells in low-density suspension culture. Original magnification, ×40. (E) Flow cytometry analysis of the frequency of apoptotic (active caspase-3⁺) cells in Nanog WT– or Nanog MT–transfected P0 cells after incubation with E7-specific CTLs. (F) Western blot analysis of expression of a panel of proapoptotic or antiapoptotic proteins in Nanog WT– or Nanog MT–transfected P0 cells. (G) Western blot analysis of Mcl-1 expression in Nanog-transfected P0 cells treated with siGFP or siRNA-targeting Mcl-1 (siMcl-1). Flow cytometry analysis of the frequency of apoptotic (active caspase-3⁺) cells in Nanog-transfected P0 cells treated with siGFP or siMcl-1 after incubation with E7-specific CTLs. (H and I) Western blot analysis of Nanog-transfected P0 cells, characterizing expression of pAkt, Akt, p21, and Mcl-1 after delivery of either (H) API2 and DMSO control or (I) Akt-specific siRNA and siGFP control. β-Actin was included as an internal loading control (A, B, and F–I). (A, B, and F–I) Numbers below blots indicate expression as measured by fold change. Error bars represent mean ± SD.

MT-transfected cells (Figure 4F). Knockdown of Mcl-1 using siRNA restored the sensitivity of Nanog-transduced tumor cells to lysis by CTLs, confirming that Mcl-1 is important for Nanog-mediated immune escape (Figure 4G). Furthermore, inhibition of the Akt pathway with API2 or siRNA diminished Mcl-1 expres-

sion by 3 or 10 fold, respectively (Figure 4, H and I), establishing a direct link between this pathway and Mcl-1. Thus, our findings demonstrate that Nanog promotes a death-resistant and stem-like phenotype in tumor cells by initiating a transcriptional program that ultimately leads to Akt-dependent upregulation of Mcl-1.

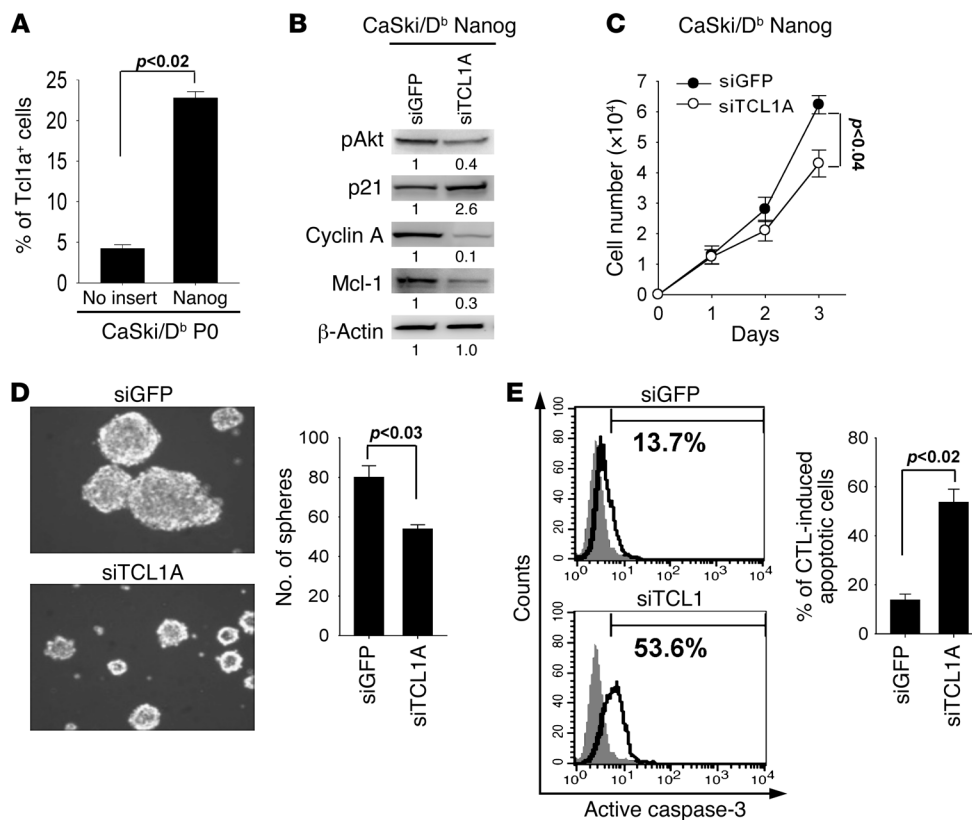


Figure 5

Nanog triggers the Akt pathway through upregulation of the Akt activator protein Tcl1a. (A) Flow cytometry analysis of the frequency of Tcl1a⁺ cells among Nanog-transfected P0 cells treated with siGFP or siTCL1A. (B) Western blot analysis of pAkt, p21, cyclin A, and Mcl-1 expression in Nanog-transfected P0 cells treated with siGFP or siTCL1A. β-Actin was included as an internal loading control. Numbers below blots indicate expression as measured by fold change. (C) Growth rate in culture of Nanog-transfected P0 cells treated with siGFP versus siTCL1A. Cells were harvested at the indicated times and counted after trypan blue staining to exclude dead cells. (D) Sphere-forming capacity of Nanog-transfected P0 cells treated with siGFP or siTCL1A in low-density suspension culture. Original magnification, ×40. (E) Flow cytometry analysis of the frequency of apoptotic (active caspase-3⁺) cells in Nanog-transfected P0 cells treated with siGFP or siTCL1A after incubation with E7-specific CTLs at a 1:1 ratio for 4 hours (isotype control staining is indicated by solid gray region; anti-active caspase-3 staining is indicated by black lines). Error bars represent mean ± SD.

Nanog triggers Akt signaling in tumor cells through transcriptional activation of Tcl1a. We next aimed to elucidate the process by which Nanog triggers the Akt pathway. The signaling molecules Eras and Pten are both known to be involved in activation of the Akt pathway (17, 18). Thus, we measured the levels of these proteins in P0 cells with and without Nanog transduction. There was no detectable change in either Eras or Pten expression after Nanog transduction (data not shown). Besides these proteins, Tcl1a has been reported as an adaptor that facilitates Akt dimerization and cross-phosphorylation, thereby initiating the Akt pathway. We therefore assessed Tcl1a expression after introduction of Nanog. Notably, the frequency of Tcl1a⁺ cells increased over 4 fold after delivery of Nanog into P0 cells (Figure 5A). To verify that Tcl1a controls activation of the Akt pathway as well as tumor phenotype in our system, we used siRNA to knockdown Tcl1a (siTCL1a) in Nanog⁺ cells and measured key biochemical and functional features of the tumor cells. siTCL1a-treated Nanog⁺ tumor cells had over 2-fold reduction in Akt phosphorylation (Figure 5B). In addition, these cells had 2.6-times

more p21, 10-times less cyclin A, and over 3-times less Mcl-1 compared with siGFP-treated Nanog⁺ tumor cells (Figure 5C). Delivery of siTCL1a also retarded proliferation, diminished sphere-forming capacity, and increased susceptibility to lysis by CTLs compared with delivery of siGFP (Figure 5, D and E). We also characterized the effect of silencing Tcl1a as well as Akt in P3 tumor cells using siRNA and observed similar results (Supplemental Figure 6). In addition, we noted that inhibition of Tcl1a or Akt reduced tumor growth in mice and rendered the tumor sensitive to lysis by CTLs (Supplemental Figures 6 and 7). These results suggest that Tcl1a acts downstream of Nanog in initiating the Akt pathway and stimulating tumor growth and survival.

This prompted us to further explore the connection between Nanog and Tcl1a. We performed qRT-PCR and found that P3 cells have 4-times more *Tcl1a* mRNA than P0 cells (Figure 6A). Also, Nanog-transduced P0 cells have 2.4-times more *Tcl1a* mRNA than empty vector-transduced P0 cells (Figure 6B). Introduction of Nanog MT cDNA, however, only led to a marginal increase in Tcl1a expression (Supplemental Figure 4C). These data show that Nanog induces upregulation of Tcl1a. We were further encouraged by the presence of Nanog-binding elements in the Tcl1a promoter region, suggesting the possibility that Nanog is a direct transcriptional activator of Tcl1a. We engineered reporter constructs containing the luciferase gene under the control of either a wild-type Tcl1a promoter (WT-Tcl1a-pGL3) or a Tcl1a promoter in which the Nanog-binding elements have been mutated (Mut-Tcl1a-pGL3) (Figure 6C). Expression of luciferase from WT-Tcl1a-pGL3 was over 3-times stronger in P3 cells compared with that in P0 cells, consistent with the abundance of Nanog⁺ cells in the P3 line (Figure 6C). Importantly, among the P3 cells, expression of luciferase was more robust from WT-Tcl1a-pGL3 than from Mut-Tcl1a-pGL3 (Figure 6C). We next performed a ChIP assay using an anti-Nanog antibody to demonstrate that Nanog associates with the Tcl1a promoter region. We successfully recovered DNA flanking the Nanog-binding elements in the Tcl1a promoter in the P3 cells and, to a lesser extent, in the P0 cells, proving that Nanog directly interacts with promoter elements upstream of the *Tcl1a* gene. Altogether, these findings establish that Nanog triggers the Akt pathway through transcriptional activation of Tcl1a.

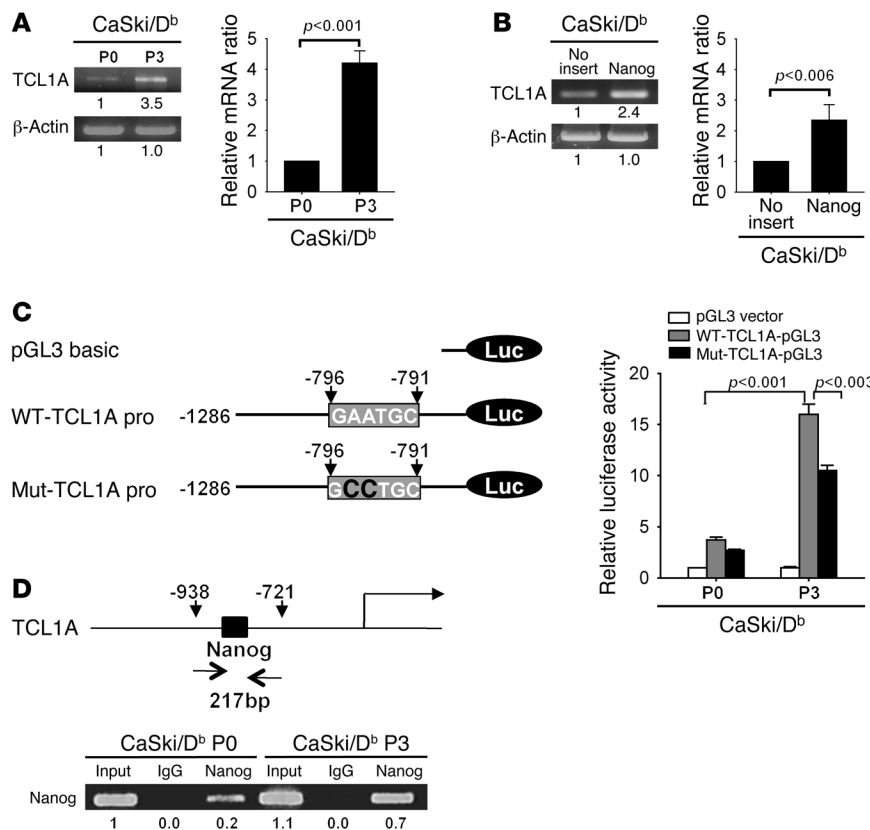


Figure 6

Nanog is a transcriptional activator of Tcl1a. (A and B) Quantitative RT-PCR analysis of *Tcl1a* mRNA expression (A) in P0 or P3 cells or (B) in P0 cells transfected with empty vector or Nanog cDNA. β-Actin was included as an internal loading control. (C) Diagram of plasmids encoding wild-type (WT) or mutant (Mut) Tcl1a promoter (nt -1,286 to +1) cloned into pGL3 vector containing the luciferase gene. In the mutant plasmid, the adenine residues in the Nanog-binding site (nt -796 to -791) have been replaced with cytosine residues to diminish Nanog binding (left). Luciferase enzymatic assay in P0 or P3 cells transfected with the indicated plasmids (right). Error bars represent mean ± SD. (D) Strategy for ChIP assay, in which a fragment corresponding to nt -938 to -721, which contains the Nanog-binding region, of the Tcl1a promoter is amplified by PCR (left). Representative gel of ChIP assay in P0 and P3 cells. Input was included as positive control, and IgG was included as negative control (right). Numbers below blots indicate expression as measured by fold change.

Nanog expression in tumor cells correlates with stage and prognosis of cervical cancer. Having unraveled the molecular mechanism by which Nanog promotes tumor growth, we aimed to determine the clinical relevance of Nanog expression in human cancer. We compared Nanog expression levels by immunohistochemistry (IHC) in cervical tissue biopsies from patients with cervical intraepithelial neoplasia (CIN) or invasive cervical carcinoma. There was an increasing amount of Nanog expression as tumor stage progressed from low-grade CIN to high-grade CIN to cancer (Figure 7, A and B). A parallel trend between expression level and disease stage was noted for Tcl1a and phosphorylated Akt (pAkt), reinforcing the link between Nanog and the Tcl1a/Akt axis (Figure 7, A and B, and Table 1). Furthermore, patients diagnosed with cervical cancer had greater Nanog, Tcl1a, and pAkt levels in tumor tissue than in nonadjacent normal tissue (Figure 7B). We next examined the relationship of Nanog expression with patients' outcomes. Kaplan-Meier plots demonstrated that patients with high Nanog expression displayed substantially worse disease-free (mean of 46.3 versus 54.6 months, $P = 0.008$) and overall (mean of 53.6 versus 57.9 months, $P = 0.015$) survival compared with that of patients with low Nanog expression (Figure 7C). These results suggest that Nanog expression may be involved in cervical cancer development and have prognostic value in patients.

We next examined the correlation in CIN or carcinoma in situ (CIS) specimens among expression of Nanog and Tcl1a and pAkt, factors we found to be critical for Nanog function. Notably, expression of Nanog was positively associated with expression of both Tcl1a ($P = 0.045$) and pAkt ($P = 0.030$), confirming that Nanog acts through the Tcl1a/Akt axis in humans (Table 2). Notably, expression of Sox2 – another protein important for

self-renewal of stem cells – was not associated with expression of Tcl1a or pAkt (Supplemental Table 1). Altogether, our data indicate that Nanog expression serves as an important prognostic factor in human cervical neoplasia.

The Nanog/Tcl1a/Akt axis is conserved across multiple cancer types. We next profiled Nanog expression across a variety of human cancer cell lines besides cervical cancer. We found Nanog at high levels in breast, lung, liver, ovarian, and colon cancer cell lines (Figure 8A). Notably, Nanog was present in 4 out of 4 colon cancer lines that we screened (Figure 8A). To verify the phenotypic effects of Nanog in these different types of cancer, we selected 3 representative lines, CUMC6, H1299, and HCT116 (from cervical, lung, and colon cancer, respectively), and performed biochemical and functional assays. Knockdown of Nanog with siRNA consistently and robustly dampened expression of Tcl1a, pAkt, cyclin A, and Mcl-1 across all tested lines (Figure 8B). Furthermore, siNanog-treated tumor cells also had diminished sphere-forming capacity and were more susceptible to immune-mediated lysis, compared with siGFP-treated tumor cells (Figure 8, C and D). These results demonstrate that overexpression of Nanog is a common feature of human cancer and that the biochemical and functional properties of the Nanog/Tcl1a/Akt signaling axis are conserved across multiple types of cancer.

Inhibition of Nanog leads to immune-mediated tumor regression in a preclinical cancer model. Because – based on our screen of a panel of human cancer lines – Nanog expression appears to be a common feature of human cancer that confers immune resistance, we reasoned that inhibition of Nanog may serve as an interventional strategy for immune-based cancer therapy. We chose to evaluate this idea in the setting of a human colon carcinoma model,



HCT116. Because HCT116 cells have not been reported to express any definitive, readily targetable tumor-associated antigens, we introduced a single-chain trimer (SCT) composed of the heavy chain of mouse MHC class I (H2-D^b), β 2-microglobulin, and the H2-D^b-restricted E7 epitope (aa 49–57) into these cells (Supplemental Figure 5A). The E7 epitope is presented on the plasma membrane by the chimeric H2-D^b, enabling the tumor cells to be recognized and killed by E7-specific CTLs (Supplemental Figure 5, B–D). Thus, use of the SCT technology allows us to effectively model immune-based therapy in the context of a prevalent tumor type characterized by high Nanog expression.

To test the therapeutic value of Nanog inhibition, we inoculated HCT116/SCT-E7 cells into NOD/SCID mice and 10 days later intravenously administered chitosan nanoparticles carrying Nanog- or GFP-targeting siRNA. Chitosan nanoparticles have been previously demonstrated to be highly efficient in delivering siRNA into the tumor mass via the enhanced permeability and retention effect (19–21). Sixteen days after tumor challenge, mice received adoptive transfer of E7-specific CTLs (Figure 9A). Delivery of siNanog elicited a profound therapeutic effect, and, when combined with adoptive transfer, the tumor was virtually undetectable, even 50 days after tumor challenge (Figure 9, B and D). Importantly, 100% of mice that received both siNanog and adoptive transfer survived, even 80 days after tumor challenge; by contrast, all the animals in the other groups had died by then (Figure 9C). Consistent with our *in vitro* results, we observed reduced levels of pAkt, Tcl1a, Mcl-1, and cyclin A, as well as elevated levels of p21, in tumor tissue from siNanog-treated mice compared with that from siGFP-treated mice (Figure 9E). Additionally, the siNanog-treated tumor contained fewer proliferating cells than the siGFP-treated tumor, as measured by Ki67 staining, and this was unaffected by adoptive transfer (Figure 9F). We assessed antigen-specific CTL infiltration into the tumor by labeling the T cells with CFSE prior to adoptive transfer and then counting the frequency of CFSE⁺ cells inside the tumor following transfer. We observed a slight, but not statistically significant, increase in the frequency of antigen-specific CTLs in the tumors of siNanog-treated mice compared with that in siGFP-treated mice (Figure 9G). However, the overall cytotoxic effect of these CTLs was greater after delivery of siNanog relative to that after delivery of siGFP, as indicated by the percentage of apoptotic tumor cells (Figure 9H). Interestingly, there was no difference in the percentage of apoptotic tumor cells in mice administered siGFP with or without adoptive transfer, suggesting that the HCT116 cells were resistant to immune-mediated control due to the presence of Nanog (Figure 9H). Taken together, our data show that inhibition of Nanog represents an attractive, widely applicable strategy for the control of human cancer, either as a sole modality or, synergistically, as part of an immune-based therapy.

Discussion

It is now generally accepted that CSCs play a prominent role in the maintenance and progression of certain cancers (9). CSCs are commonly spared and thus enriched by conventional forms of cancer therapy, such as radiation or pharmacologic agents (22–25). However, the relationship between CSCs and the host immune system is largely unknown. We previously demonstrated in a mouse model that vaccination drives the evolution of tumor cells toward a phenotype resembling CSCs in a process requiring

Nanog, a transcription factor pivotal in self-renewal of embryonic stem cells (14). It was unclear at the time whether the emergence of stem-like Nanog⁺ tumor cells was a general consequence of immune selection or merely an artifact of the particular vaccination system we used. To address this issue, here we used *in vitro* immune selection, in which the cells are directly pulsed with antigen and then exposed in sequential rounds to antigen-specific CTLs, to generate human cancer cells. The result of such a selection process was, after 3 rounds, a line of tumor cells, P3, that were almost completely impervious to lysis by CTLs. This P3 line thus enabled us to study the molecular signatures that facilitate development of immune escape. The P3 line had a stem-like and highly tumorigenic phenotype. Strikingly, we also found that nearly 100% of the P3 cells had abundant Nanog expression and that the stem-like phenotype of these cells was critically dependent on Nanog. Since we have demonstrated this with 2 distinct selection methods, we infer that Nanog⁺ tumor cells may also be enriched by naturally occurring adaptive immune surveillance. Nonetheless, all of our experiments thus far have been conducted with externally imposed selection techniques, so it is plausible that this model might not apply to physiological host-tumor interactions in the absence of any interventions that modulate the status of the immune system. Nonetheless, the evidence we have is sufficient to conclude that enhancement of a stem-like tumor phenotype through Nanog is a general outcome of imposed immune selection, regardless of the mechanism by which such selection is brought forth (Figure 10A).

It is important to note that Nanog⁺ tumor cells in P3 cells are not equivalent to conventional CSCs. Indeed, while virtually all P3 cells had Nanog expression, only a small fraction of these cells stained positive for various stemness markers. There is currently no broad consensus about the precise molecular definition of CSCs, hampering our ability to accurately quantify the number of CSCs in the P3 line compared with its parent line, P0. However, based on the widely accepted hallmarks of CSCs — namely, sphere-forming capacity, tumorigenicity, and expression of stemness markers — we consistently observed that the P3 population exhibited more of a stem-like phenotype relative to the P0 population. It is reasonable to posit a model in which Nanog, in conjunction with other factors (which may or may not be present within individual cells), promotes the conversion of tumor cells into CSCs, as has been proposed (8, 26–28). As we and others have shown (14, 29, 30), besides its ability to turn tumor cells into CSCs, Nanog also confers a growth and survival benefit. Therefore, immune selection favors Nanog⁺ cells, and a fraction of these cells contain the accessory factors necessary to be fully reprogrammed into bona fide CSCs. The detailed molecular events involved in the conversion of tumor cells into CSCs are still shrouded in mystery. Our focus in this study was to shed light on the pathway by which Nanog acts to bring about the stem-like and immune-resistant phenotype of tumor cells.

In this vein, we uncovered the Tcl1a/Akt signaling axis as the downstream component triggered by the transcriptional function of Nanog. Notably, after depletion of Tcl1a or Akt, the stem-like and immune-resistant phenotype of P3 cells or Nanog-transduced P0 cells was almost entirely lost, indicating that the Akt pathway is the primary route through which Nanog acts to promote this phenotype. Moreover, we did not detect any influence of Nanog on expression or activation of p38 or Erk, although we cannot exclude possible contributions from other signaling cascades. Our

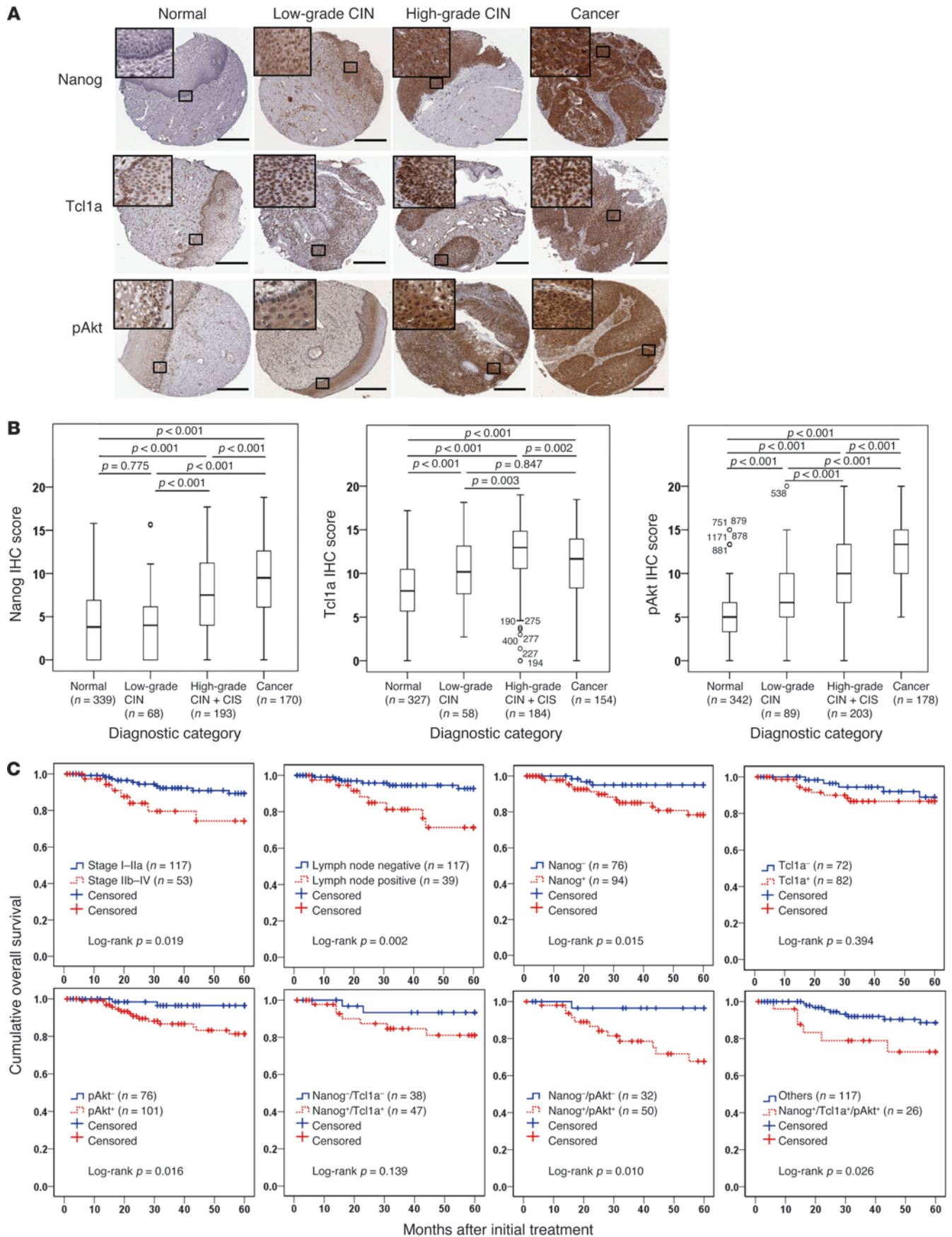




Figure 7

Nanog expression in human cervical neoplasia specimens correlates with stage and outcome of disease. **(A)** Representative image of immunohistochemical staining of Nanog, Tcl1a, and pAkt expression in cervical tissue from patients with low-grade CIN, high-grade CIN, and cervical carcinoma. Boxed regions are displayed at high magnification in insets (scale bar: 200 μ m). **(B)** Box plot depiction of IHC data. The IHC score is an index of Nanog, Tcl1a, or pAkt expression and was computed based on intensity and tissue area of positive staining. In box-and-whisker plots, horizontal bars indicate the medians, boxes indicate 25th to 75th percentiles, and whiskers indicate the lowest and highest datum within 1.5 interquartile range of the lower and upper quartiles, respectively. Symbols indicate individual samples. Numbers associated with symbols indicate case numbers. **(C)** Kaplan-Meier plots for patients with cervical cancer stratified according to FIGO stage, lymph node metastasis, or Nanog, Tcl1a, or pAkt expression. For patients with high Nanog expression, mean disease-free and overall survival were 46.3 months and 53.6 months ($n = 94$), respectively. For patients with low Nanog expression, mean disease-free and overall survival were 54.6 months and 57.9 months ($n = 76$), respectively.

discovery of the pathway through which Nanog acts is significant because it links a master regulator of stem cells to a major signaling axis often exploited by tumor cells. This connection immediately hints at several potentially promising therapeutic targets to control cancer in the clinic (Figure 10B).

Indeed, we found that Nanog expression was elevated in multiple types of human cancer and depletion of Nanog reduced the stem-like character of tumor cells and rendered them more vulnerable to lysis by CTLs. Furthermore, Nanog expression in tumor tissue correlated with stage and outcome of disease in patients with cervical neoplasia. These data underscore the value of Nanog expression as a prognostic factor in cervical neoplasia and strongly suggest that the functions of Nanog on tumor cells that we observed in vitro hold true in patients with cancer as well. Importantly, Nanog expression in precancerous cervical tissue was correlated with both Tcl1a and pAkt expression, validating the biochemical pathway we proposed. It is also notable that Nanog expression correlated with resistance of cervical tumors to chemotherapy, such as the platinum-based agent cisplatin (Supplemental Table 2). Previous reports further found Akt activation to be associated with cisplatin resistance in various types of tumor, including those of the uterine cervix (31–34). Therefore, it will be important in future studies to assess involvement of the Nanog/Tcl1a/Akt axis in promoting tumor resistance to chemotherapy.

Individuals with productive HPV infection frequently mount a robust immune response against the E6 and E7 HPV antigens. In fact, 90% of individuals who test positive for HPV will clear the virus within 6 to 24 months. Moreover, spontaneous regression occurs in 60% to 80% of people with HPV-associated, low-grade CIN, and only 1% eventually advance to cervical CIS. Escape of the tumor from immune control is believed to be an essential step in the development of cervical cancer (35). As evidence of this, patients with high frequencies of tumor-infiltrating CTLs typically have no detectable lymph node metastasis and have a good prognosis (36, 37). Furthermore, patients with late-stage cervical cancer usually possess a high amount of regulatory T cells and a low amount of natural killer cells (38). Our data suggest that, in addition to immune escape, acquisition of intrinsic immune resistance by tumor cells through the Nanog/Tcl1a/Akt pathway may also be important in the progression of cervical neoplasia. We

found the degree of Nanog expression to be positively correlated with disease stage and outcome in patients with cervical neoplasia. Taken together, our results provide insight into the events that occur at the level of tumor cells in the onset and development of cervical cancer.

Due to the stem-like and immune-resistant phenotype mediated by Nanog across multiple types of human cancer, this protein represents a prime target for therapeutic intervention. We provided proof of this concept by knocking down Nanog in a xenograft mouse model of human colon cancer. Notably, in this setting, Nanog inhibition alone strongly retarded tumor growth and, when combined with adoptive transfer of tumor-specific CTLs, virtually cured animals of disease. As we understand more and more about CSCs and their sinister role in tumor progression, metastasis, and relapse, it is increasingly clear that cancer therapy should also be directed against this rare but robust population of cells in order to provide meaningful, long-term benefit to patients. As we have demonstrated here, Nanog inhibition appears to be an ideal strategy for achieving this, particularly in the context of immune-based therapy.

Methods

Mice. 6- to 8-week-old female NOD/SCID mice (Central Lab Animal Inc.) were maintained and handled under a protocol approved by the Korea University Institutional Animal Care and Use Committee (KUIA-CUC-2009-126). All procedures were performed in accordance with recommendations for the proper animal care and use.

DNA constructs. To generate pMSCV/Nanog, cDNA encoding human Nanog was amplified from pSIN-EF2-Nanog-Pur (Addgene) using primer set 5'-GCCTCGAGATGAGTGTGGATCCAGCTTG-3' (forward) and 5'-GCGAATTCTCACACGTCTTGAGGTTG-3' (reverse). The amplified cDNA was cloned into *XhoI/EcoRI* restriction sites of the pMSCV retroviral vector (Clontech). The promoter region of the *Tcl1a* gene was isolated by PCR from genomic DNA extracted from CaSki/D^b P3 cells using primer set 5'-GGGGTACCTCTGTGGCTATCTAGGTCT-3' (forward) and 5'-AATAAGCTTCTTGGGGCGGGACCCCGGT-3' (reverse). The PCR products were digested with *KpnI* and *HindIII* and subcloned into the *KpnI/HindIII* restriction sites of the pGL3-Basic vector (Promega). To generate pMSCV/SCT-E7, a DNA fragment encoding the H2-D^b-restricted E7 epitope (aa 49–57) and flanked by *AgeI* and *NheI* restriction sites was synthesized by annealing 2 single-stranded DNA oligonucleotides: 5'-CCGGAGAGCCATTACAATATTGTAACCTTT-3' and 5'-CTAGTCTCGGGTAATGTTATAACATTGAAA-3'. This fragment was then subcloned into the *AgeI/NheI* restriction sites of the pIRES-E6-2m-Kb plasmid reported previously (39) to swap the E6 antigen with E7 and produce pIRES-E7-2m-Kb. H2-D^b heavy chain DNA was amplified by PCR using TC-1 cDNA templated and cloned into pIRES-E7-2m-Kb to replace H2-K^b with H2-D^b. Finally, E7-2m-Db was amplified with PCR, using pIRES-E7-Db as the template, and subsequently cloned into the *BglII/XhoI* sites of pMSCV (Clontech). In all cases, plasmid integrity was confirmed by DNA sequencing.

Site-directed mutagenesis. The QuikChange XL Site-Directed Mutagenesis Kit was used (Stratagene) according to the manufacturer's instructions. To create mutations in the *Nanog* gene, the following primers were used: E264G, 5'-TGCCAGTGACTTGGGGGCTGCGTGGAAG-3' (forward) and 5'-CTTCCAAGGCAGCCCCAAGTCACTGGCA-3' (reverse); E268G, 5'-GAGGCTGCCTTGGGAGCTGCTGGGGAA-3' (forward) and 5'-TTCCCCAGCAGCTCCAAGGCAGCGC-3' (reverse); E272A, 5'-GGAAGCTGCTGGGCGAGCCCTAATGTAA-3' (forward) and 5'-TTACATTAAGGCTGCCCCAGCAGCTTCC-3' (reverse). To create



Table 1

Univariate and multivariate analyses of the association between prognostic variables and overall survival in cervical cancer

	Univariate analysis		Multivariate analysis	
	Hazard ratio (95% CI)	P value	Hazard ratio (95% CI)	P value
FIGO stage (≥IIb)	3.39 (1.27–9.06)	0.015	1.52 (0.43–5.27)	0.507
Tumor grade (poor)	2.10 (0.81–5.46)	0.124		
Tumor size (>4 cm)	1.56 (0.59–4.10)	0.365		
LVI	2.20 (0.72–6.74)	0.166		
LN metastasis	4.14 (1.43–11.96)	0.009	4.11 (1.19–14.17)	0.025
Nanog ⁺	4.41 (1.26–15.40)	0.020	5.80 (1.26–26.51)	0.023
Tcl1a ⁺	1.67 (0.56–4.98)	0.358		
pAkt ⁺	5.10 (1.15–22.45)	0.031	4.21 (1.18–14.91)	0.026
Nanog ⁺ /Tcl1a ⁺	2.74 (0.92–8.16)	0.070		
Nanog ⁺ /pAkt ⁺	6.28 (1.72–22.85)	0.005	6.79 (1.85–24.92)	0.004
Nanog ⁺ /Tcl1a ⁺ /pAkt ⁺	3.04 (1.08–8.56)	0.056	4.37 (1.40–21.33)	0.012

LVI, lymphatic vessel invasion; LN metastasis, lymph node metastasis.

mutations in the Nanog-binding site of Tcl1a, the following primers were used: 5'-GCCTTAGTGGGCTGCGTTACTGCAAAATAAAGT-GAAATTGT-3' (forward) and 5'-CAGTAACGCAGGCCCACTAAGG-CAATTAAGAAAGTCATGCA-3' (reverse). Thermal cycling conditions for PCR were 95°C for 1 minute; 18 cycles of 95°C for 50 seconds, 60°C for 50 seconds, and 68°C for 7 minutes; and 68°C for 7 minutes. PCR products were digested with *DpnI* at 37°C for 1 hour and transformed into XL10-Gold ultracompetent bacterial cells (Stratagene). Mutations were verified by DNA sequencing.

siRNA constructs. Synthetic siGFP, siNanog, and siTcl1a (Invitrogen) had the following sequences: GFP, 5'-GCAUCAAGGUGAACUCAA-3' (sense), 5'-UUGAAGUUCACCUUGAUGC-3' (antisense); Nanog, 5'-GCAACCAGACCUGGAACAAU-3' (sense), 5'-UUGUCCAGGUCUGGUUGCUU-3' (antisense); and Tcl1a, 5'-GCCCUUAACCAUCGA-GAUA-3' (sense), 5'-UAUCUCGAUGGUUAAGGGC-3' (antisense). siAkt (no. 6211) was purchased commercially (Cell Signaling Technology). siRNA was delivered in vitro into 6-well plates at a dose of 300 pmol per well using Lipofectamine 2000 (Invitrogen). siRNA was delivered into mice after formulation with chitosan nanoparticles as described previously (20). Briefly, tripolyphosphate (0.25% w/v) and siRNA (1 µg/µl) were combined in RGd-chitosan solution, and the mixture was incubated at 4°C for 40 minutes. siRNA-loaded nanoparticles were purified by centrifugation and injected into the tail veins of HCT116/SCT-E7 tumor-bearing mice.

Cells. CaSki, CUMC6, MCF7, MDA-MB-231, MDA-MB-453, H1299, HepG2, OVCAR3, SKOV3, A2780, HT29, SNUC4, SW620, and HCT116 cells were obtained commercially (ATCC). CaSki, CUMC6, MCF7, MDA-MB-231, MDA-MB-453, HepG2, SNUC4, SW620, and HCT116 cells were cultured in Dulbecco's Minimal Eagle Medium (DMEM). H1299, OVCAR3, SKOV3, and A2780 were cultured in RPMI1640. All cells were cultured at 37°C in 5% CO₂ atmosphere.

Generation of the CaSki-D^b P3 tumor line. CaSki-D^b P0 cells were produced by retroviral transduction of CaSki cells with pMSCV/H2-D^b using pMSCV vector-Phoenix packaging cell line system, followed by puromycin selection, as described previously (40). For immune selection, 10⁶ CaSki-D^b cells were pulsed with 1 µg E7 peptide (aa 49–57, RAHY-NIVTF) for 2 hours and mixed with 10⁶ mouse E7-specific CTLs (1:1 ratio) for 4 hours in 10 ml DMEM in a 50-ml

conical tube supplemented with 10% FBS and penicillin/streptomycin (50 U/ml). Surviving CaSki-D^b cells were further cultured in the presence of puromycin (10 mg/ml) to deplete CTLs. Expanded cells were termed P1 cells. The above procedure was repeated twice to create the P3 line.

Tumor sphere-forming assay. CaSki-D^b P0 or P3 cells were plated at 5 × 10³ cells per well in 6-well, super-low adherence vessels (Corning) containing serum-free DMEM-F12 (Thermo Scientific) supplemented with epidermal growth factor (20 ng/ml), basic fibroblast growth factor (20 ng/ml), and 1XB27. Medium was replaced every 3 days to replenish nutrients. Colonies more than 2 mm in diameter were counted under a microscope.

Tumorigenicity assay. CaSki-D^b P0 or P3 cells were harvested by trypsin treatment and then washed and resuspended in Opti-MEM. NOD/SCID mice were subcutaneously injected with 10³ or 10⁴ P0 or P3 cells. Tumor formation was monitored at least 3 times per week. After 18 days, tumor tissue was excised and weighed.

Real-time quantitative RT-PCR. Total RNA from CaSki-D^b P0 or P3 cells was purified using TRIzol reagent (Invitrogen). First-strand synthesis and real-time PCR were performed and quantified by LightCycler 1.5 (Roche) to detect *Tcl1a* mRNA using TaqMan Universal SYBR Green Master Mix (Roche) with the following primer set: 5'-GCCTGGGAGAAAGTTCGT-GTA-3' (forward) and 5'-TCAGTCATCTGGCAGCAGC-3' (reverse).

Immunofluorescence microscopy. CaSki-D^b P0, P1, P2, or P3 cells were fixed

Table 2

Association between Nanog and Sox2, Tcl1a, or pAkt expression in CIN and CIS

	Nanog expression				n	P value
	Low	%	High	%		
Sox2 expression					151	0.007
Low	25	80.6	6	19.4	31	
High	65	54.2	55	45.8	120	
Tcl1a expression					149	0.045
Low	15	78.9	4	21.1	19	
High	71	54.6	59	45.4	130	
pAkt expression					182	0.030
Low	52	67.9	25	32.1	78	
High	54	51.9	50	48.1	104	

Numbers in the "Low" and "High" columns refer to the number of samples meeting each condition. Numbers in the "n" column indicate the total number of samples tested for each condition.

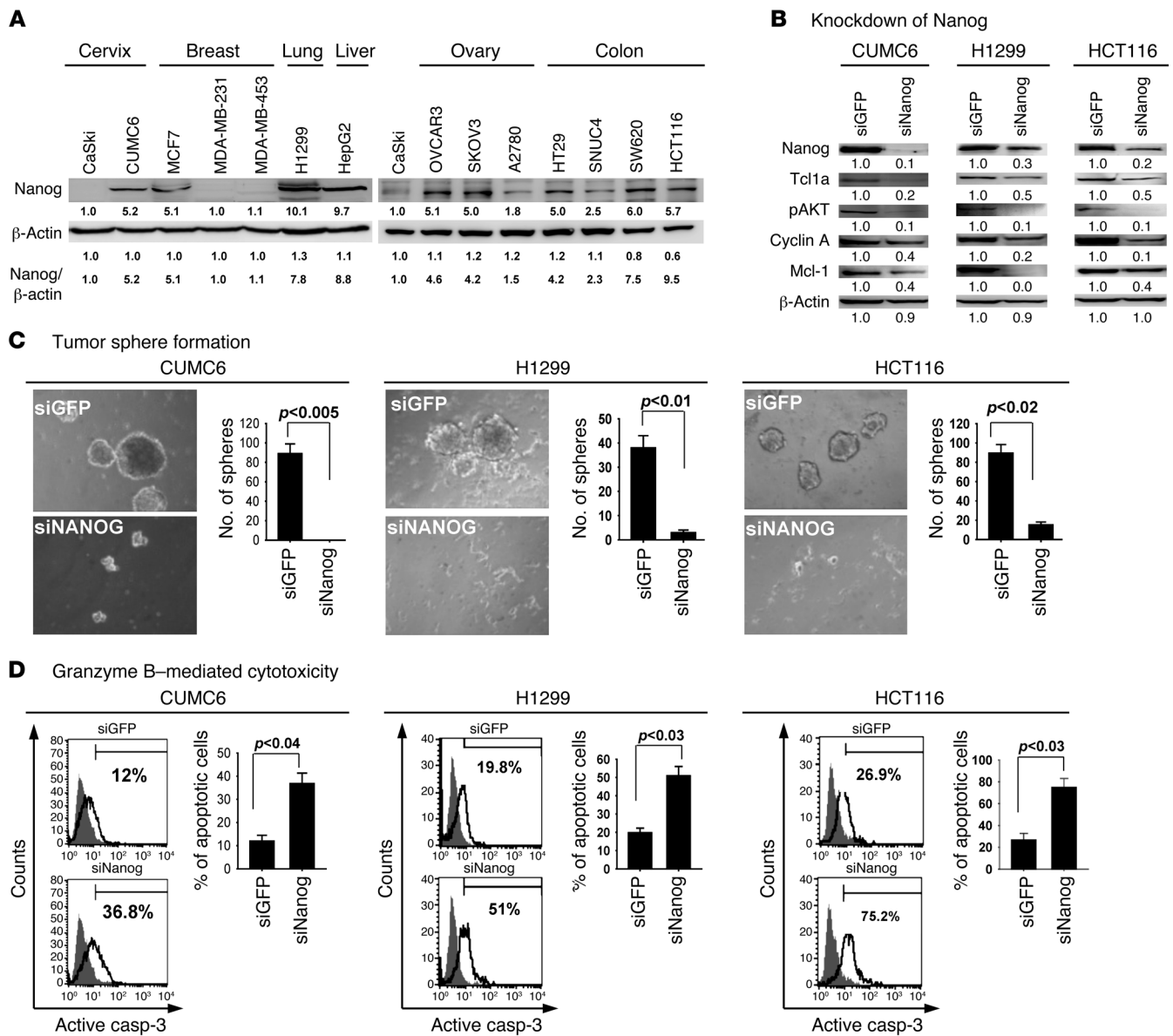


Figure 8

Nanog promotes a stem-like and immune-resistant phenotype in multiple types of human cancer. **(A)** Western blot analysis of Nanog expression in various human cancer lines. β-Actin was included as an internal loading control. **(B)** Western blot analysis of expression of Nanog, Tcl1a, pAkt, cyclin A, and Mcl-1 in human cancer cells treated with siGFP or siNanog. β-Actin was included as an internal loading control. **(A and B)** Numbers below blots indicate expression as measured by fold change. **(C)** Sphere-forming capacity of human cancer cells treated with siGFP or siNanog in low-density suspension culture **(D)** Flow cytometry analysis of the frequency of apoptotic (active caspase-3⁺) cells in human cancer cells treated with siGFP or siNanog after incubation with E7-specific CTLs at a 1:1 ratio for 4 hours (isotype control staining is indicated by solid gray region; anti-active caspase-3 staining is indicated by black lines). Original magnification, ×40. Error bars represent mean ± SD.

in 4% paraformaldehyde for 10 minutes. Cells were washed with PBS and treated with 0.2% Triton X-100 and blocked for 1 hour in 1% BSA solution. Cells were incubated overnight with primary antibodies against Nanog (Millipore) and then stained with Alexa Fluor 488-labeled goat anti-mouse IgG and DAPI. Expression of Nanog was analyzed by confocal laser scanning microscopy (Carl Zeiss) as described previously (41).

Western blot. Lysate extracted from a total of 10⁵ cells was used to perform Western blot as described previously (42). Primary antibodies against pAkt, Akt, pErk, Erk, Tcl1a, Eras, Pten, Bcl-xL, cIAP2, Bad, Bax, c-Myc,

Cdk2, cyclin A, and cyclin E (Cell Signaling Technology); cIAP2, Mcl-1, Bcl-2, Oct4, Sox2, Klf4, and p21 (Santa Cruz Biotechnology Inc.); Nanog (Millipore); and β-actin (Sigma-Aldrich) were used at 1:1,000 dilution. Immune-reactive bands were visualized by enhanced chemiluminescence imaging (Elpis Biotech).

CTL assay. CaSki/Db P0, P1, P2 and P3 tumor cells were harvested by trypsinization, washed once with DMEM (Hyclone) containing 0.1% FBS, resuspended, and labeled in 1 ml 0.1% FBS containing DMEM and 10 μM CFSE. The suspended cells were incubated for 10 minutes in a 37°C

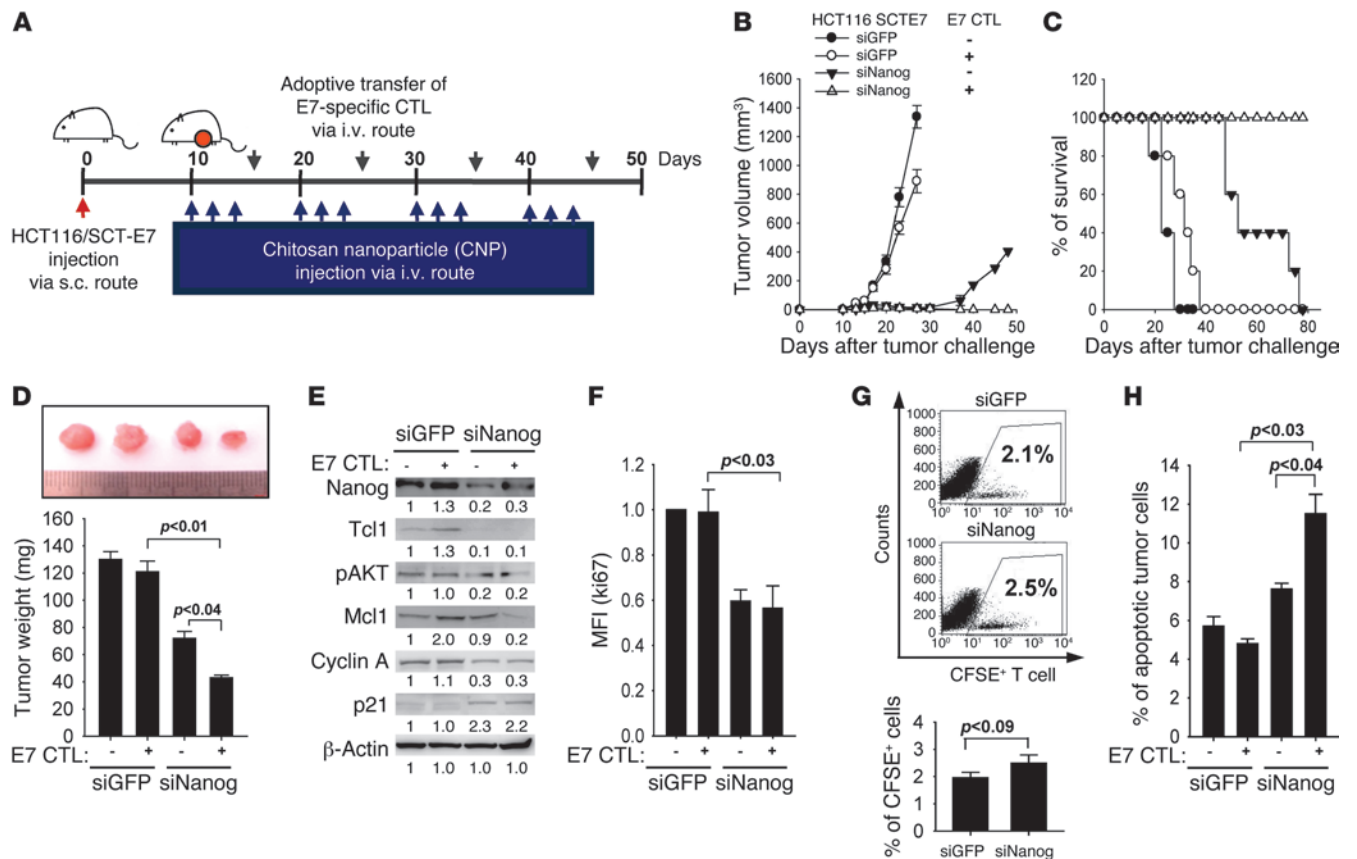


Figure 9
 Inhibition of Nanog renders the tumor vulnerable to immune-mediated control. (A) Diagram of the immune-based therapy regimen in mice implanted with HCT116 colon cancer cells transduced with plasmid encoding a SCT of H2-D^b heavy chain linked to β2-microglobulin and the H2-D^b-restricted E7 epitope (HCT116/SCT-E7). (B) Tumor growth and (C) survival of mice inoculated with HCT116/SCT-E7 and treated with the indicated reagents (5 mice/group). (D) Tumor mass of mice at 25 days after challenge. (E) Western blot analysis of Nanog, pAkt, Tcl1a, Mcl-1, cyclin A, and p21 expression in mice administered with siGFP or siNanog, with or without adoptive transfer of E7-specific CTLs. β-Actin was included as an internal loading control. Numbers below blots indicate expression as measured by fold change. (F) Flow cytometry analysis of the proliferation index of cells inside the tumor, as measured by the mean fluorescence intensity of Ki67 staining. (G) Flow cytometry analysis of the frequency of CFSE-labeled, E7-specific CTLs in the tumors of mice that received adoptive transfer, together with either siGFP or siNanog. (H) Flow cytometry analysis of the frequency of apoptotic (active caspase-3⁺) cells in the tumors of siGFP- or siNanog-treated mice, with or without adoptive transfer of E7-specific CTLs. Error bars represent mean ± SD.

incubator with 5% CO₂. After collection, the CFSE-labeled cells were resuspended in 10 μg/ml E7 peptide containing 1 ml DMEM. After 1 hour, CFSE-labeled CaSki/Db P0, P1, P2, and P3 cells were incubated for 4 hours with an E7-specific CD8⁺ T cell line at an E/T ratio of 1:1. After incubation for 4 hours at 37°C, the frequency of apoptotic cells was determined by staining with anti-active caspase-3 antibody and performing flow cytometry as described previously (43, 44).

Granzyme B apoptosis assays. Human granzyme B (Enzo Life Sciences) was introduced into cells with the BioPORTER QuikEase Protein Delivery Kit (Sigma-Aldrich). 5 × 10⁴ cells per well were plated in 24-well plates and cultured overnight at 37°C. Cells were washed, and 200 ng of granzyme B in Opti-MEM was added to each well. After incubation for 4 hours at 37°C, the frequency of apoptotic cells was determined by staining with anti-active caspase-3 antibody and performing flow cytometry as described previously (14).

Flow cytometry analysis. CaSki/Db P0, P1, P2, and P3 tumor cells were harvested by trypsinization, washed, and resuspended in PBS. To detect CD133, CD166, CD44, and EpCAM expression, primary antibody incubation was applied for 1 hour at 4°C and rinsed, and then secondary antibody was

applied for 30 minutes at 4°C. Antibodies used were CD133 (1:100; Abcam), CD166 (1:100; BD Pharmingen), CD44 (1:50; Cell Signaling Technology), and EpCAM (1:50; Abcam). Secondary antibodies (1:200) used were either goat anti-rabbit IgG or goat anti-mouse IgG labeled with Alexa 568 (Molecular Probes), respectively. All data acquisition was performed on a FACSCalibur flow cytometer (BD Biosciences) with CellQuest Pro software.

Luciferase enzymatic assay. CaSki-D^b P0 and P3 cells were maintained in DMEM with 10% FBS and seeded at 10⁵ cells per well in 12-well plates 1 day prior to the assay. Cells were administered using Lipofectamine 2000 (Invitrogen) with 500 ng WT- or Mut-Tcl1a-pGL3 reporter, together with 50 ng CMV/β-galactosidase plasmid to normalize transfection efficiency. After 24 hours, cells were washed with PBS and permeabilized with Cell Culture Lysis Reagent (Promega). Luciferase activity was measured with a Turner Biosystems TD-20/20 luminometer after addition of 40 μl luciferase assay reagent (Promega). β-Galactosidase activity was measured with a uQuant microplate reader (BioTek) at 570-nm wavelength after addition of β-galactosidase assay reagent containing 1 mM chlorophenol red β-D-galactopyranoside substrate (Roche).

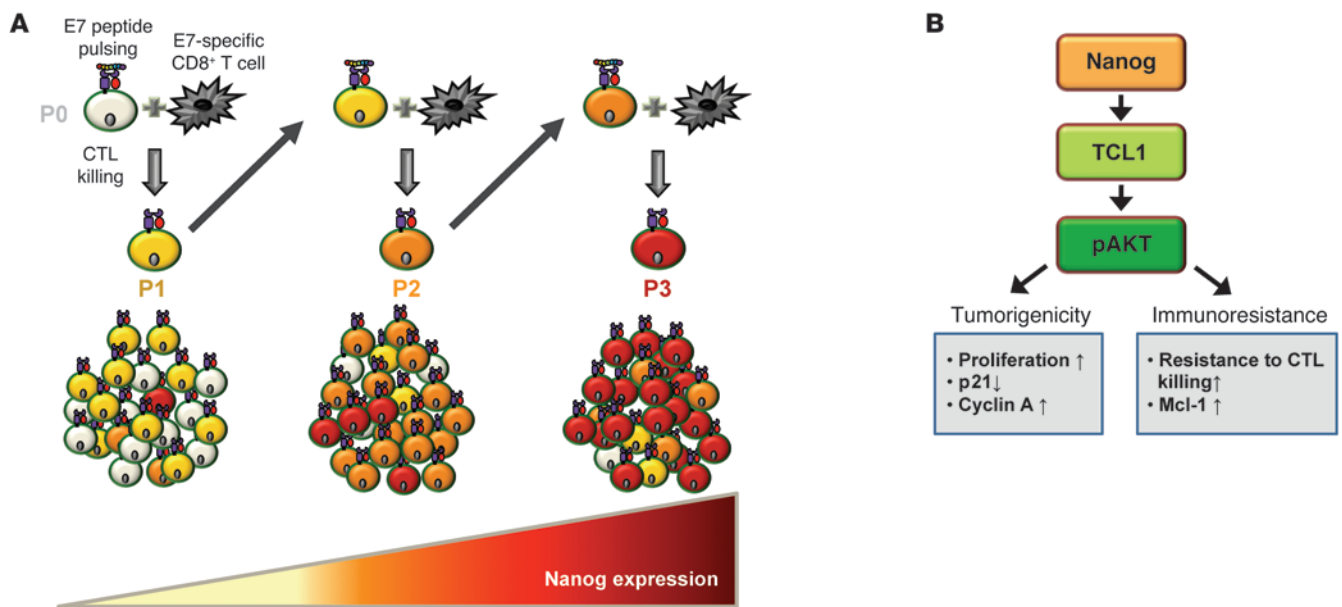


Figure 10 Model depicting the role of Nanog in cancer progression and immune escape. **(A)** Enrichment of Nanog-expressing cells through sequential rounds of immune selection. **(B)** The molecular pathway through which Nanog promotes tumorigenicity and immune resistance of tumor cells.

ChIP assay. The ChIP Kit (Millipore) was used according to the manufacturer's instructions. Briefly, CaSki-D^b P0 and P3 cells (10^7 per assay) were bathed in 1% formaldehyde at 25°C for 10 minutes for cross-linking of proteins and DNA and then lysed in SDS buffer containing 1× protease inhibitor. DNA was sheared to 0.2- to 1-kb fragments by sonication using a Sonic Dismembrator Model 500 (Fisher Scientific). Immunoprecipitation was carried out by incubation with 2 μg anti-Nanog antibody (Millipore) or mouse IgG (Upstate Biotechnology) as a negative control for 16 hours. To reverse the protein-DNA crosslinks, immunoprecipitated sample and input were incubated at 65°C for overnight. After reversal of cross-linking, DNA fragments were purified on spin columns (Upstate Biotechnology). The region flanking the Nanog-binding site in the Tcl1a promoter was amplified by PCR from purified chromatin with the following primers: 5'-ATGTTCTTAGTGCCTGGTCAG-3' (forward) and 5'-ATGATCAAACCACCCCTCTGTA-3' (reverse). The PCR product was resolved on a 2% agarose gel containing ethidium bromide and visualized under ultraviolet light.

Tumor treatment experiments. NOD/SCID mice were inoculated subcutaneously with 10^6 HCT116/SCT-E7 cells per animal and administered siNanog- or siGFP-loaded chitosan nanoparticles (5 μg/animal) via the tail vein at days 10, 12, and 14. Sixteen days after tumor challenge, mice received adoptive transfer with 10^7 E7-specific CTLs. This treatment protocol was repeated for 3 cycles at days 20, 30, and 40. Mice were monitored for tumor burden and survival for 50 and 80 days after challenge, respectively.

Human subjects. The study subjects consisted of 431 patients diagnosed with CIN ($n = 193$), CIS ($n = 68$), or cervical cancer ($n = 170$) after primary surgery at Gangnam Severance Hospital, Yonsei University College of Medicine, between 1996 and 2010. All patients were diagnosed histologically, and disease was classified according to the International Federation of Gynecology and Obstetrics (FIGO) system. Medical records were reviewed to collect pertinent data, including age, disease stage, lymphovascular invasion, lymph node metastasis, platinum reagent resistance, survival status, and tumor differentiation, type, and size. Patients

with cervical cancer received adjuvant platinum-based concurrent chemoradiation therapy to reduce risk of relapse. This study was approved by the Institutional Review Boards of Gangnam Severance Hospital and the Office of Human Subjects Research at the NIH.

Tissue microarray construction and IHC. Tissue microarray (TMA) were produced from formalin-fixed, paraffin-embedded tumor and nonadjacent normal cervical tissue. Some of the paraffin blocks were provided by the Korea Gynecologic Cancer Bank through the Bio & Medical Technology Development Program of the Ministry of Education, Science and Technology. Areas representative of CIN, CIS, or cervical cancer were meticulously selected from H&E-stained slides. Tissue cylinders of 1.0-mm diameter were extracted from selected areas of donor blocks and transplanted into recipient blocks using a tissue arrayer (Beecher Instruments Inc.). H&E-stained TMA slides were examined at every 50th section for the presence of tumor cells. For IHC, all paraffin sections were cut to 5-μm thickness, deparaffinized through xylene, and dehydrated with graded ethanol. Antigen retrieval for Nanog, Sox2, Tcl1a, and pAkt was performed in a pressure cooker containing prewarmed citrate buffer at pH 9.0 (Dako) for 10 minutes. Endogenous peroxidase activity was blocked by addition of 3% H₂O₂ for 10 minutes. Samples were incubated with primary antibodies against Nanog (1:100 dilution), Sox2 (1:500 dilution) (Cell Signaling Technology), Tcl1a (1:1,000 dilution) (Millipore), and pAkt (1:500 dilution) (Abcam) for 2 hours at 25°C. Samples stained for Nanog, Tcl1a, and pAkt were then incubated with EnVision Dual Link secondary antibody for 30 minutes, and samples stained for Sox2 were incubated with high-sensitivity EnVision FLEX linker and horseradish peroxidase antibody for 15 minutes (Dako). Samples were then developed by addition of 3,3'-diaminobenzidine substrate for 10 minutes and lightly counterstained with hematoxylin.

Digital image analysis. IHC-stained whole TMA sections were processed into digital format at ×20 magnification using an Aperio Scanscope CS (Aperio). The Scanscope acquired each image with a spatial resolution of 0.50 μm per pixel and an average file size of 220 MB. Each image was



reviewed with Digital Image Hub software (SlidePath) to annotate regions of normal or tumor tissue. The image was then subjected to automated analysis by Tissue IA (SlidePath). Within Tissue IA, an algorithm was invented to quantify Nanog expression based on intensity, concentration, and tissue area of positive staining. These parameters were combined to assign an IHC score of 0 to 20 to each sample, resembling minimal to maximal levels of expression, respectively.

Statistics. All data are representative of at least 3 separate experiments. Individual data points were compared by 2-tailed Student's *t* test. IHC scores were compared by nonparametric 1-way analysis of variance and independent *t* test. Correlation of Nanog with Tc1a, Sox2, and pAkt expression was evaluated with χ^2 test. Immunohistochemical cut-off for high expression of markers was determined through the receiver operating characteristic (ROC) curve analysis. The sensitivity and specificity for discriminating death or life was determined at each IHC score and plotted, thus generating a ROC curve. The cut-off value was established to be the point on the ROC curve in which the sum of sensitivity and specificity was maximized. Kaplan-Meier survival analysis was performed to determine the association of Nanog expression and disease-free or overall survival, and survival curves between groups were compared with log-rank test. Univariate and multivariate analysis of hazard ratios for death were performed using the Cox proportional regression model. Analysis was performed with SPSS version 12.0 software. In all cases, *P* < 0.05 was considered statistically significant.

Study approval. All animal procedures were performed under a proto-

col approved by the Korea University Institutional Animal Care and Use Committee (KUIACUC-2009-126). Human studies received informed consent from participants and were approved by the institutional review boards of Gangnam Severance Hospital and the Office of Human Subjects Research at the NIH.

Acknowledgments

This work was supported by funding from the National Research Foundation of Korea (2012-007527, 2011-0027588, and 2011-0002608), the Korea Healthcare Technology R&D Project (A062260), and the United States National Cancer Institute (P50 CA098252 and RO1 CA114425). The authors thank Katherine Liu for the preparation of the manuscript.

Received for publication April 10, 2012, and accepted in revised form August 16, 2012.

Address correspondence to: T.-C. Wu, Department of Pathology, Johns Hopkins School of Medicine, CRB II Room 309, 1550 Orleans Street, Baltimore, Maryland 21231, USA. Phone: 410.614.3899; Fax: 443.287.4295; E-mail: wutc@jhmi.edu. Or to: Tae Woo Kim, Division of Infection and Immunology, Graduate School of Medicine, Korea University, 516 Gojan-1 Dong, Ansan-Si, Gyeonggi-Do 425-707, Seoul, Republic of Korea. Phone: 82.31.412.6713; Fax: 82.31.412.6718; E-mail: twkim0421@korea.com.

1. Siegel R, Naishadham D, Jemal A. Cancer Statistics, 2012. *Ca-a Cancer Journal for Clinicians*. 2012;62(1):10-29.
2. Wilczynski JR, Duechler M. How do tumors actively escape from host immunosurveillance? *Arch Immunol Ther Exp (Warsz)*. 2010;58(6):435-448.
3. Hanahan D, Weinberg RA. Hallmarks of cancer: the next generation. *Cell*. 2011;144(5):646-674.
4. Hanahan D, Weinberg RA. The hallmarks of cancer. *Cell*. 2000;100(1):57-70.
5. Schatton T, Frank MH. Antitumor immunity and cancer stem cells. *Ann N Y Acad Sci*. 2009; 1176:154-169.
6. Frank NY, Schatton T, Frank MH. The therapeutic promise of the cancer stem cell concept. *J Clin Invest*. 2010;120(1):41-50.
7. Dean M, Fojo T, Bates S. Tumour stem cells and drug resistance. *Nat Rev Cancer*. 2005;5(4):275-284.
8. Lee TK, Castilho A, Cheung VC, Tang KH, Ma S, Ng IO. CD24(+) liver tumor-initiating cells drive self-renewal and tumor initiation through STAT3-mediated NANOG regulation. *Cell Stem Cell*. 2011;9(1):50-63.
9. Dalerba P, Cho RW, Clarke MF. Cancer stem cells: models and concepts. *Annu Rev Med*. 2007; 58:267-284.
10. Ma S, Lee TK, Zheng BJ, Chan KW, Guan XY. CD133+ HCC cancer stem cells confer chemoresistance by preferential expression of the Akt/PKB survival pathway. *Oncogene*. 2008;27(12):1749-1758.
11. Visvader JE, Lindeman GJ. Cancer stem cells in solid tumours: accumulating evidence and unresolved questions. *Nat Rev Cancer*. 2008;8(10):755-768.
12. Zhou BB, Zhang H, Damelin M, Geles KG, Grindley JC, Dirks PB. Tumour-initiating cells: challenges and opportunities for anticancer drug discovery. *Nat Rev Drug Discov*. 2009;8(10):806-823.
13. Singec I, et al. Defining the actual sensitivity and specificity of the neurosphere assay in stem cell biology. *Nat Methods*. 2006;3(10):801-806.
14. Noh KH, et al. Cancer vaccination drives Nanog-dependent evolution of tumor cells towards an immune-resistant and stem-like phenotype. *Cancer Res*. 2012;72(7):1717-1727.
15. Oh JH, et al. Identification of a putative transactivation domain in human Nanog. *Exp Mol Med*. 2005;37(3):250-254.
16. Do HJ, et al. Two potent transactivation domains in the C-terminal region of human NANOG mediate transcriptional activation in human embryonic carcinoma cells. *J Cell Biochem*. 2009;106(6):1079-1089.
17. Lee MY, Lee SH, Park JH, Han HJ. Interaction of galectin-1 with caveolae induces mouse embryonic stem cell proliferation through the Src, ERas, Akt and mTOR signaling pathways. *Cell Mol Life Sci*. 2009;66(8):1467-1478.
18. Vanhaesebroeck B, Stephens L, Hawkins P. PI3K signalling: the path to discovery and understanding. *Nat Rev Mol Cell Biol*. 2012;13(3):195-203.
19. Han HD, et al. Targeted gene silencing using RGD-labeled chitosan nanoparticles. *Clin Cancer Res*. 2010;16(15):3910-3922.
20. Han HD, et al. A chitosan hydrogel-based cancer drug delivery system exhibits synergistic antitumor effects by combining with a vaccinia viral vaccine. *Int J Pharm*. 2008;350(1-2):27-34.
21. Lu C, et al. Regulation of tumor angiogenesis by EZH2. *Cancer Cell*. 2010;18(2):185-197.
22. Zielske SP, Spalding AC, Wicha MS, Lawrence TS. Ablation of breast cancer stem cells with radiation. *Transl Oncol*. 2011;4(4):227-233.
23. Wu Y, Wu PY. CD133 as a marker for cancer stem cells: progresses and concerns. *Stem Cells Dev*. 2009;18(8):1127-1134.
24. Ginestier C, et al. CXCR1 blockade selectively targets human breast cancer stem cells in vitro and in xenografts. *J Clin Invest*. 2010;120(2):485-497.
25. Wu A, et al. Persistence of CD133+ cells in human and mouse glioma cell lines: detailed characterization of GL261 glioma cells with cancer stem cell-like properties. *Stem Cells Dev*. 2008;17(1):173-184.
26. Chiou SH, et al. Coexpression of Oct4 and Nanog enhances malignancy in lung adenocarcinoma by inducing cancer stem cell-like properties and epithelial-mesenchymal transdifferentiation. *Cancer Res*. 2010;70(24):10433-10444.
27. Brandner S. Nanog, Gli, and p53: a new network of stemness in development and cancer. *EMBO J*. 2010;29(15):2475-2476.
28. Machida K, et al. Toll-like receptor 4 mediates synergism between alcohol and HCV in hepatic oncogenesis involving stem cell marker Nanog. *Proc Natl Acad Sci U S A*. 2009;106(5):1548-1553.
29. Chiou SH, et al. Coexpression of Oct4 and Nanog enhances malignancy in lung adenocarcinoma by inducing cancer stem cell-like properties and epithelial-mesenchymal transdifferentiation. *Cancer Res*. 2010;70(24):10433-10444.
30. Jeter CR, et al. Functional evidence that the self-renewal gene NANOG regulates human tumor development. *Stem Cells*. 2009;27(5):993-1005.
31. Yang X, Fraser M, Moll UM, Basak A, Tsang BK. Akt-mediated cisplatin resistance in ovarian cancer: modulation of p53 action on caspase-dependent mitochondrial death pathway. *Cancer Res*. 2006;66(6):3126-3136.
32. Wei LH, et al. The anti-apoptotic role of interleukin-6 in human cervical cancer is mediated by up-regulation of Mcl-1 through a PI 3-K/Akt pathway. *Oncogene*. 2001;20(41):5799-5809.
33. Wu HH, et al. cIAP2 upregulated by E6 oncoprotein via epidermal growth factor receptor/phosphatidylinositol 3-kinase/AKT pathway confers resistance to cisplatin in human papillomavirus 16/18-infected lung cancer. *Clin Cancer Res*. 2010;16(21):5200-5210.
34. Arafa el SA, et al. Tangeretin sensitizes cisplatin-resistant human ovarian cancer cells through down-regulation of phosphoinositide 3-kinase/Akt signaling pathway. *Cancer Res*. 2009;69(23):8910-8917.
35. Tindle RW. Immune evasion in human papillomavirus-associated cervical cancer. *Nat Rev Cancer*. 2002;2(1):59-65.
36. Piersma SJ, et al. High number of intraepithelial CD8+ tumor-infiltrating lymphocytes is associated with the absence of lymph node metastases in patients with large early-stage cervical cancer. *Cancer Res*. 2007;67(1):354-361.
37. Eerola AK, Soini Y, Paakko P. A high number of tumor-infiltrating lymphocytes are associated with a small tumor size, low tumor stage, and a favorable prognosis in operated small cell lung car-



- cinoma. *Clin Cancer Res.* 2000;6(5):1875-1881.
38. Patel S, Chiplunkar S. Host immune responses to cervical cancer. *Curr Opin Obstet Gynecol.* 2009;21(1):54-59.
39. Huang CH, et al. Cancer immunotherapy using a DNA vaccine encoding a single-chain trimer of MHC class I linked to an HPV-16 E6 immunodominant CTL epitope. *Gene Ther.* 2005;12(15):1180-1186.
40. Noh KH, et al. Activation of Akt as a mechanism for tumor immune evasion. *Mol Ther.* 2009;17(3):439-447.
41. Kang TH, Kim KW, Bae HC, Seong SY, Kim TW. Enhancement of DNA vaccine potency by antigen linkage to IFN-gamma-inducible protein-10. *Int J Cancer.* 2011;128(3):702-714.
42. Kim JH, et al. Enhancement of dendritic cell-based vaccine potency by anti-apoptotic siRNAs targeting key pro-apoptotic proteins in cytotoxic CD8(+) T cell-mediated cell death. *Immunol Lett.* 2009;122(1):58-67.
43. Kang TH, et al. Ectopic expression of X-linked lymphocyte-regulated protein pM1 renders tumor cells resistant to antitumor immunity. *Cancer Res.* 2010;70(8):3062-3070.
44. Kang TH, et al. Epigallocatechin-3-gallate enhances CD8+ T cell-mediated antitumor immunity induced by DNA vaccination. *Cancer Res.* 2007;67(2):802-811.